

COMPARATIVE ANALYSIS OF A SOLAR TRIGENERATION SYSTEM BASED ON PARABOLIC TROUGH COLLECTORS USING GRAPHENE AND FERROFLUID NANOPARTICLES

by

Alla IBRAHIM^{a*} and Muhammet KAYFECI^b

^a Department of Mechanical Engineering, Graduate School of Natural and Applied Sciences,
Karabuk University, Karabuk, Turkey

^b Department of Energy Systems Engineering, Faculty of Technology,
Karabuk University, Karabuk, Turkey

Original scientific paper
<https://doi.org/10.2298/TSCI191103164I>

In this comparative study, the thermodynamic analysis of a trigeneration system driven by a parabolic through solar collector based on two different types of nanofluid is performed. A standard trigeneration system consists of two subsystems, including an absorption heat pump and the organic Rankine cycle. Two types of nanoparticles (graphene and ferrofluid) that possess excellent and diverse physical properties within a base fluid (Syltherm 800) were selected to be the absorption fluids in the solar cycle. Four organic fluids, namely R123, R401a, R601, and R601a, for the organic Rankine cycle are examined. The results clearly depicted improvement in the system performance. It was found that graphene nanoparticles performed better as compared to the ferrofluid nanoparticles. The largest temperature of the collector outlet was obtained at 257.4 °C with Syltherm 800/graphene. The highest net power produced by the system was 134.1 kW and the maximum overall energy and exergy efficiencies of the system were 160.5% and 21.84%, respectively. The highest net power produced by the system was 134.1 kW and the maximum overall energy and exergy efficiencies of the system were 160.5% and 21.84%, respectively. The solar collectors are the main source of the exergy destruction and the highest value was recorded about 683 kW.

Key words: solar collector, trigeneration, nanofluids, energy, exergy

Introduction

Solar power generation technology is one of the emerging sciences due to the extensive availability of solar power, economical power generation, and environment-friendly impact of solar power. Thus, this source of energy is the best choice for exploiting among the existing RES [1]. Moreover, the design of innovative high performance systems is a critical issue that attracts much attention. Many solar systems are used for generating electricity, which includes parabolic through solar collector (PTSC), solar dishes, and towers [2]. The PTSC is the best-known solar thermal technology for power generation [3] and it has been used in large power plants since the early 1980's. The efficiency of conventional power plants is generally low. Therefore, the integration between cooling and heating systems in the existing plants can substantially improve the plant efficiency. The implementation of this additional step is known as trigeneration, which involves power generation, cooling, and heating at the

* Corresponding author, e-mail: alariefi@yahoo.com

same time [4]. It appears that the combination of solar systems and trigeneration systems is ideal when a rich source of efficient renewable energy is used. Experts have solved the problem of low thermal and optical performance experienced in solar energy conversion systems by using nanofluids as a working fluid in solar-thermal systems. This has been viewed as an innovative approach to improve the thermal performance of the power generation systems, thus making them more sustainable. Nanofluids represent a new class of modern heat transfer fluids, which are designed to disperse nanoparticles smaller than 100 nm in conventional heat transfer fluids [5]. So far, only a few studies have been conducted on solar energy use as the main energy source in trigeneration systems, especially in the cases, in which, nanofluids are used as working fluids.

Ceylan and Ergun [6] designed a new PTSC as a temperature control. They found that the new collector can provide hot water with low solar radiation and its costs are cheaper than other systems. Bellos *et al.* [7] conducted a study, in which, they tried four solar collector types including evacuated tube collectors, flat plate collectors, PTSC, and compound parabolic collectors for providing the best solution to run refrigeration appliances. The LiBr-H₂O was applied as a working fluid for the absorption cooling system. According to the researchers, the four systems' comparative analysis shows that PTSC acted as an optimal exergetic system. Kaya *et al.* [8] carried out an experimental assessment to find out the effects of adding nanofluid into neat methanol on the energy and exergy efficiencies of a concentrated air collector with vacuum tube heat pipe. Experimental results had shown that using nanofluid within the base fluid had positive effect on the performance of the system. The effects of using nanofluids in a solar dish collector (SDC) or a PTSC on the multi-generation system had been studied by Abid *et al.* [9]. They declared that the PTSC systems outperformed as compared to the SDC systems in terms of power generation. Moreover, they achieved 23.8% exergy efficiency using the PTSC system while 23.25% with the SDC system. During their experiments, Toghiani *et al.* [10] utilized certain nanofluid types to operate the Rankine cycle by a PTSC system. They found that the dispersion of CuO, TiO₂, Al₂O₃, and SiO₂ nanoparticles in the thermal oil could improve the system's exergy efficiencies by 3%, 6%, 11%, and 9%. Alashkar and Gadalla [11] studied the use of nanofluid-based solar PTSC to operate the Rankine cycle. They achieved a slight increase in the annual energy output using Syltherm 800 and Therminol VP-1 with the Cu, Al₂O₃, and SWCNT. Bellos and Tzivanidis [12] evaluated a trigeneration system driven by nanofluid-based PTSC. Cyclohexane, n-octane, toluene, and octamethyltrisiloxane were applied as working fluids in the organic Rankine cycle (ORC) when Al₂O₃ and CuO nanoparticles dissolved in the base fluid (Syltherm 800) of a solar system. They found that toluene with CuO nanoparticles was the optimal combination. Alashkar and Gadalla [13] tested nanofluids including Syltherm 800 and Therminol VP-1 with Cu and Ag in a PTSC to run the Rankine cycle. Their findings show that the annual energy production rose by 11.7%.

An experimental study conducted by Alsaady *et al.* [14] throws light on the ferrofluid effect on the efficiency of a parabolic trough collector. They found that using ferrofluids in the solar collectors showed environmental benefits, improvements in heat transfer, and reductions in the required area for heat transfer. Khosravi *et al.* [15] conducted a study that showed excellent optical thermal conversion performance of solar collectors under specific conditions when magnetic nanofluids were used. The results showed that magnetic nanofluids significantly absorb solar radiation and improve solar collector efficiency. Pop *et al.* [16] examined the specific heat and thermal conductivity of graphene nanoparticles. They indicated that the strange thermal properties of graphene come from its 2-D nature, shaping a rich area for new discoveries

tics. The purpose of the AHP is cooling by supplying chilled water. Moreover, it has the capacity to run heating applications by supplying hot water. The system's output energy can be utilized for heating. This energy is equal to the heat that a condenser and absorber reject during the cycle. While the extracted heat from the medium by the evaporator can be utilized for cooling applications.

Table 1. Thermal properties of the examined nanoparticles and base fluid [19, 20]

Nanoparticle	ρ [kgm ⁻³]	C_p [Jkg ⁻¹ K ⁻¹]	K [Wm ⁻¹ K ⁻¹]	μ [kgm ⁻¹ s ⁻¹]
Graphene	2160	710	5000	–
Ferrofluid	5200	670	6	–

Table 2. Examined organic fluids in the ORC [21, 22]

Organic fluid type	Molar mass [kgkmol ⁻¹]	Critical temperature [°C]	Critical pressure [MPa]	Ozone depletion potential	Global warming potential (100 year)
R601	72.15	196.54	3.37	0	20
R123	152.93	183.76	3.66	0.02	77
R141b	116.95	204.34	4.21	0.12	725
R601a	72.15	187.2	3.38	0	20

Mathematical modeling

The current section presents the mathematical modeling of the integrated system. The system comprises of an AHP, the ORC, and some parabolic trough collectors. The following equations have been formulated and EES software has been used to solve them. Table 3 shows the input data, which is used for coding.

Table 3. Input data used in the analysis

Parameters	Values	Parameters	Values
Solar beam irradiation	960 W/m ²	Glass cover outer diameter	125 mm
Sun temperature	5770 K	Glass cover emittance	0.90
Collector aperture area	69.2 m ²	Nanoparticles volume concentration	6%
Volumetric flow rate on the PTSC	3 m ³ /h	Wind speed	1 m/s
Receiver inner diameter	66 mm	Optical efficiency	74.1%
Receiver outer diameter	70 mm	The ORC turbine efficiency	85%
Glass cover inner diameter	120 mm	The ORC pump efficiency	70%

The parabolic trough solar collector

The PTSC analysis has been presented in the current section, which is formulated according to the equations given in a study by Kalogirou [23]. The thermal efficiency, η_c , of a PTSC is actually useful energy, Q_u , which is divided by the total incident radiation, G_B . The activity takes place on an aperture plane, A_a , therefore:

$$\eta_c = \frac{\dot{Q}_u}{A_a G_B} \quad (1)$$

The useful energy that is delivered from a concentrator is calculated:

$$\dot{Q}_u = \dot{m}_{nf} C_{p,nf} (T_{out} - T_{in}) \quad (2)$$

where $C_{p,nf}$ is the specific heat of nanofluids. The T_{out} and T_{in} , represent the solar collectors' outlet and inlet temperatures, respectively, while \dot{m}_{nf} represents the nanofluids' mass-flow rate inside the receiver. The useful energy has also been calculated:

$$\dot{Q}_u = F_R [G_B \eta_o A_a - A_r U_L (T_{in} - T_{amb})] \quad (3)$$

where F_R represents heat removal factor:

$$F_R = \frac{\dot{m}_{nf} C_{p,nf}}{A_r U_L} \left[1 - \exp \left(- \frac{U_L \dot{F} A_r}{\dot{m}_{nf} C_{p,nf}} \right) \right] \quad (4)$$

Receiver area $A_r = \pi D_{r,0} L$. The efficiency factor of the collector, \dot{F} will be:

$$\dot{F} = \frac{\frac{1}{U_L}}{\frac{1}{U_L} + \frac{D_{r,0}}{h_{fi} D_{r,i}} + \left(\frac{D_{r,0}}{2k_r} \ln \frac{D_{r,0}}{D_{r,i}} \right)} = \frac{U_0}{U_L} \quad (5)$$

where $D_{r,0}$ stands for the receiver tube's outer diameter, $D_{r,i}$ – the inner diameter, U_0 – the total heat transfer coefficient, k_r – the receiver tube's thermal conductivity, and h_{fi} – the convective heat transfer coefficient. The nanofluids have thermo physical properties, including thermal density, specific heat, and conductivity, which are calculated through eqs. (6)-(9) [24, 25].

$$\rho_{nf} = \varphi \rho_{np} + (1 - \varphi) \rho_{bf} \quad (6)$$

$$C_{p,nf} = \frac{\varphi(\rho_{np} C_{p,np}) + (1 - \varphi)(\rho_{bf} C_{p,bf})}{\rho_{nf}} \quad (7)$$

$$K_{nf} = K_f \frac{K_{np} + 2K_{bf} + 2(K_{np} - K_{bf})(1 + \beta)^3 \varphi}{K_{np} + 2K_{bf} - (K_{np} - K_{bf})(1 + \beta)^3 \varphi} \quad (8)$$

$$\mu_{nf} = \mu_{bf} (1 + 2.5\varphi + 6.5\varphi^2) \quad (9)$$

The β value indicates the ratio between the nanolayer thickness and the initial radius of the particle. Typically, this parameter is specified to be 0.1 [26]. The concentration of nanoparticle volume has a definitive impact on the nanofluids' thermal properties, which is illustrated in fig. 2. It is obvious that increasing the nanoparticles' concentration increases dynamic viscosity, density, and thermal conductivity of a nanofluid, however, its specific thermal efficiency decreases. This mainly happens because of the fact that the base fluid (Syltherm 800) has a higher specific heat capacity than the nanoparticles and vice versa for other thermal properties. It can also be observed that a graphene-based nanofluid has the highest

specific heat capacity and thermal conductivity while a ferrofluid has the highest density. Moreover, the dynamic viscosity is the same for both the nanofluids.

Thus the overall heat loss coefficient in the collector will be:

$$U_L = \left[\frac{A_r}{A_g (h_w + h_{r,c-a})} + \frac{1}{h_{r,r-c}} \right]^{-1} \quad (10)$$

where A_g and A_r are the outer glass cover area and the outer receiver area, respectively.

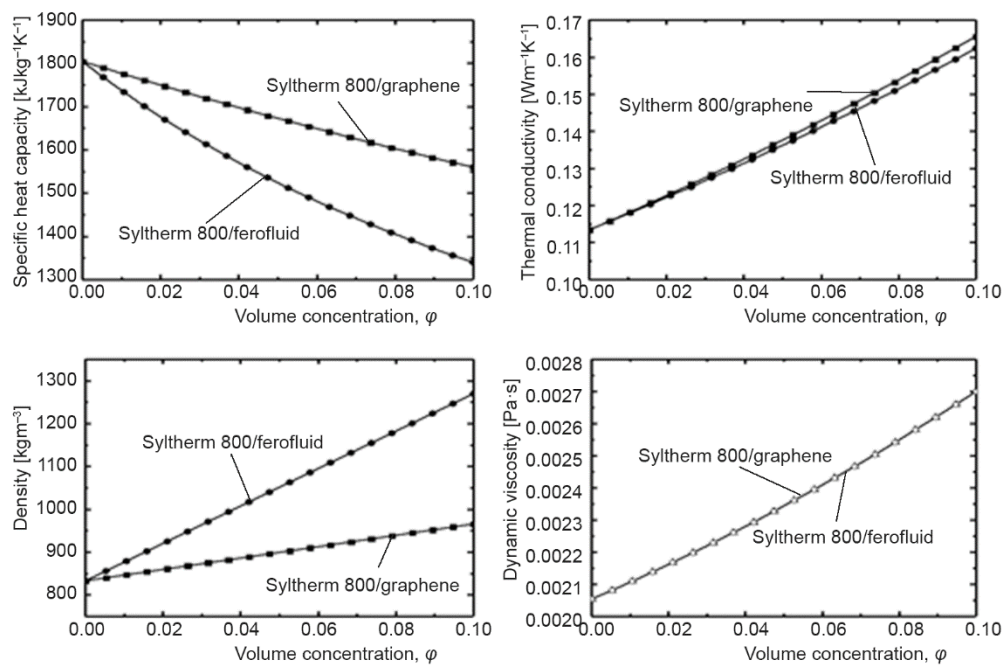


Figure 2. Effect of nanoparticle volume concentration on the thermal properties of nanofluids

For the number of solar collectors, N , the total available solar irradiation is:

$$Q_{\text{sol}} = A_a G_B N \quad (11)$$

The efficiency of the collector can be computed by:

$$\eta_c = \frac{F_R}{N} \left[\eta_o - U_L \left(\frac{T_i - T_{\text{amb}}}{G_B \frac{A_a}{A_r}} \right) \right] \quad (12)$$

The difference between E_{in} and E_{out} is the exergy destruction in the PTSC. The entropy generation rate can be expressed:

$$S_{\text{gen,PTSC}} = \frac{1}{T_0} (E_{\text{in}} - E_{\text{out}}) \quad (13)$$

The absorption heat pump and organic Rankine cycle

Both the First and the Second thermodynamics laws have been utilized for every part of the subsystems by assuming the appropriate parameters [27]. The simulation and analysis process of the trigeneration system includes computing the energy and exergy balance equations based on the assumptions given to each component. The ORC, η_{ORC} , energy efficiency will be:

$$\eta_{ORC} = \frac{w_{tur} - w_p}{\dot{Q}_{in}} \quad (14)$$

The ORC system's exergy efficiency can be calculated by:

$$\eta_{ex,ORC} = \frac{w_{net}}{\dot{Q}_{eva} \left(1 - \frac{T_{amb}}{T_{eva}} \right)} \quad (15)$$

The AHP performance coefficient for cooling can be given:

$$COP_{cooling} = \frac{\dot{Q}_{eva}}{\dot{Q}_{gen}} \quad (16)$$

The AHP performance coefficient for cooling is written:

$$COP_{heating} = \frac{\dot{Q}_{cond} + \dot{Q}_{abs}}{\dot{Q}_{gen}} = 1 + COP_{cooling} \quad (17)$$

The AHP exhibits exergy efficiency, which can be expressed:

$$\eta_{ex,cooling} = \frac{\dot{Q}_{eva} \left(1 - \frac{T_{amb}}{T_{eva}} \right)}{\dot{Q}_g \left(1 - \frac{T_{amb}}{T_{gen}} \right)} \quad (18)$$

The AHP shows heat exergy efficiency, which can be calculated:

$$\eta_{ex,heating} = \frac{\dot{Q}_{cond} \left(1 - \frac{T_{amb}}{T_{cond}} \right) + \dot{Q}_{abs} \left(1 - \frac{T_{amb}}{T_{abs}} \right)}{\dot{Q}_g \left(1 - \frac{T_{amb}}{T_{gen}} \right)} \quad (19)$$

Overall system

The system's energy efficiency can be obtained by dividing the useful output energy by the input energy:

$$\eta_{en,system} = \frac{\dot{W}_{net} + \dot{Q}_{eva} + \dot{Q}_{abs} + \dot{Q}_{cond}}{\dot{Q}_{sol}} \quad (20)$$

The system performance can be best analyzed through computing its exergy efficiency because that takes into account the useful output, and it is determined through the following equation:

$$\eta_{\text{ex,system}} = \frac{\dot{W}_{\text{net}} + \dot{Q}_{\text{eva}} \left(\frac{T_{\text{amb}}}{T_{\text{eva}}} \right) + \dot{Q}_{\text{abs}} \left(1 - \frac{T_{\text{amb}}}{T_{\text{abs}}} \right) + \dot{Q}_{\text{cond}} \left(1 - \frac{T_{\text{amb}}}{T_{\text{cond}}} \right)}{\dot{E}x_{\text{solar,in}}} \quad (21)$$

where $\dot{E}x_{\text{solar,in}}$ represents the solar systems inlet exergy, which is calculated using:

$$\dot{E}x_{\text{solar,in}} = \dot{Q}_{\text{sol}} \left[1 - \frac{4}{3} \left(\frac{T_{\text{amb}}}{T_{\text{Sun}}} \right) + \frac{1}{3} \left(\frac{T_{\text{amb}}}{T_{\text{Sun}}} \right)^4 \right] \quad (22)$$

Results and discussion

The current section presents and discusses the numerical analysis and the solar-driven trigeneration system simulation using the mathematical models presented in the previous section. The analyses were performed using the EES software under steady-state conditions. Initially, the performance parameters were calculated for thermodynamic analysis of the base case of the integrated solar-trigeneration system according to fig. 1. This was followed by the variable parameters, which were separately tested to determine their impact on the performance of the trigeneration system. The mentioned variables include energy efficiency, net electrical power output, total exergy destruction rate, exergy efficiency, heating and cooling, and component exergy destruction value.

Table 4. Most important parameters of the solar system analysis with different working fluids

Description	Syltherm 800/graphene	Syltherm 800/ferrofluid	Syltherm 800
$T_{\text{out}} [^{\circ}\text{C}]$	257.4	245.8	256.6
$\eta_c [\%]$	73.37	73.44	73.31
$\dot{Q}_u [\text{kW}]$	783.3	783.7	782.6
$\dot{E}x_{\text{solar,in}} [\text{kW}]$	674.3	683	675.2
$\rho [\text{kgm}^{-3}]$	875.7	1065	819.5
$C_p [\text{Jkg}^{-1}\text{K}^{-1}]$	1705	1514	1830
$K [\text{Wm}^{-1}\text{K}^{-1}]$	0.1602	0.1566	0.1106
$\mu [\text{kgm}^{-1}\text{s}^{-1}]$	0.001548	0.001664	0.001746
$\dot{m} [\text{kgs}^{-1}]$	0.7298	0.8867	0.6829
$S_{\text{gen}} [\text{Wm}^{-1}\text{K}^{-1}]$	438.5	443.9	438.9
$h_{\bar{t}} [\text{Wm}^{-2}\text{K}^{-1}]$	628.4	671.9	467.8

The solar system performance with different absorption fluid types is listed in tab. 4, which compares two types of nanofluids and the base fluid. The highest PTSC outlet temperature is obtained using Syltherm 800/graphene as the working fluid in the solar cycle at

257.4 °C. This result was obtained due to the graphene nanoparticles having the relatively high thermal capacity and thermal conductivity while they have relatively lower density. The rate of entropy generation was determined keeping in view friction and heat transfer of the working fluid in the receiver tube. The results show that the solar system with Syltherm 800/graphene had the lowest entropy generation rate (approximately 438.5 W/mK), thereby making it less irreversible. This means that the process in that cycle involves the smallest temperature difference and the smallest irreversibility (entropy generation rate) [27]. Furthermore, it becomes clear that adding nanoparticles to the absorption fluid positively affects the solar system. The convective heat transfer coefficient and mass flow rate increase in the PTSC receiver using nanoparticles.

The results acquired are general due to the assumptions applied in analyzing the models. The results of the current model were confirmed and validated by the reference models [9, 23]. The comparison results are shown in tab. 5. The subsystems performance for all organic fluid-working fluid combinations in the solar cycle is listed in tab. 6. The R601, R601a, R123, and R141b were tested for the ORC cycle and two types of nanofluid were examined for the solar system, including Syltherm 800/graphene, Syltherm 800/ferrofluid, and thermal oil (Syltherm 800). According to the mentioned table, the highest overall energy value and exergy efficiency are acquired when Syltherm 800/graphene was applied as an absorption fluid and working fluid R601a was used for ORC (160.5% and 21.84%, respectively). Note that the energy efficiency value is greater than 100%, which was expected. For cooling and heating purposes, AHP is used. A cooling load acts as an input to the system, and it can be converted into useful thermal energy production source by using rejected heat from the absorber and the condenser for heating. These results show good agreement with the results of theoretical studies conducted by Bellos and Tziva-

Table 5. Validation results for the PTSC

Material	η_e [%]
[23]	72.5
Fe ₂ O ₃ -water [9]	73.09
Molten salt [9]	72.08
Syltherm 800/ferrofluid (This study)	73.44
Syltherm 800 (This study)	73.31

Table 6. Subsystems performance using different working fluids

Nanofluid	Syltherm 800/ferrofluid				Syltherm 800/graphene				Syltherm 800			
	Description	R601	R123	R141b	R601a	R601	R123	R141b	R601a	R601	R123	R141b
w_{net} [kW]	127.6	60.62	75.91	129.3	132.5	62.9	78.86	134.1	132.2	62.75	78.66	133.7
$\eta_{en,ORC}$ [%]	25.67	25.67	25.1	27.14	26.54	26.42	25.77	28.07	26.48	26.37	25.73	28.01
$\eta_{ex,ORC}$ [%]	7.336	6.837	6.304	7.878	8.092	4.478	6.936	8.683	8.041	7.435	6.894	8.629
COP _{cooling}	0.758	0.771	0.777	0.755	0.749	0.762	0.771	0.748	0.749	0.763	0.772	0.748
$\eta_{ex,cooling}$ [%]	19.53	22.68	25.19	18.92	17.54	20.41	22.55	17.05	17.67	20.55	22.71	17.16
COP _{heating}	1.758	1.771	1.777	1.755	1.749	1.762	1.771	1.748	1.749	1.763	1.772	1.748
$\eta_{ex,heating}$ [%]	40.43	46.47	51.34	39.26	36.61	42.13	46.22	35.63	36.84	42.39	46.53	35.85
$\eta_{en,svstem}$ [%]	141.5	92	80.95	144.8	158.2	109	99.82	160.5	157.2	108	98.61	159.6
$\eta_{ex,svstem}$ [%]	20.11	10.99	11.78	20.48	21.55	12.18	13.15	21.84	21.46	12.11	13.06	21.67
$\dot{E}_{XD,total}$ [kW]	853.7	794.9	795.1	847.7	863.4	801.5	802.1	856.5	863	801.3	801.9	856.2

Table 7. Validation of the results of the proposed system

Material	w_{net} [kW]	$\eta_{en. ORC}$ [%]	$COP_{cooling}$	$\eta_{en. svstem}$ [%]	$\eta_{ex. svstem}$ [%]
Therminol VP-1, R601, [28]	58.66	10.11	0.7718	175.9	20.55
Syltherm 800, Cyclohexane, [12]	139.9	18.82	0.697	141.3	23.29
Syltherm 800/graphene, R601, this study	132.5	26.54	0.749	158.2	21.55
Syltherm 800, R601, this study	132.2	26.48	0.748	157.2	21.46

midis [28] as shown in tab. 7. From the results shown in tab. 6, it can also be noted that using the mentioned working fluids, the highest values of electricity production, and ORC exergy and energy efficiencies are obtained. This result has a reason: the PTSC exit temperature was the highest when Syltherm 800/graphene was used as compared to other absorption fluids. The best absorption system performance has been obtained using Syltherm 800/ferrofluid and R141b, with COP for cooling and heating 0.777 and 1.777, respectively. The exergetic absorption system efficiencies for heating and cooling were 51.43 and 25.19, respectively.

A comparison is made between usage of different nanofluids in the solar system and usage of different organic fluids in the ORC, as shown in tab. 6. The system's overall exergetic destruction remained the lowest when Syltherm 800/ferrofluid and R123 were used at approximately 794.9 kW. This can be justified by the fact that ferrofluid nanoparticles have relatively low specific heat capacity and very high density, which reduces the energy needs for increasing temperature. The exergy destruction is an indication of whether the system performs well or not. In other words, detecting the high exergy destruction source and its reduction can help improving the system's overall performance.

Table 8 shows the value of the exergy destruction of the main components in the proposed system for different absorption fluid types in the solar system. The results are presented here for the organic fluid R601 because it showed the highest exergy destruction values. The exergy destruction is an indication of whether the system performs well or not. In other words, detecting the high exergy destruction source and reducing it can help improve

Table 8. Exergy Destruction values for the main components of the proposed system [kW]

Component	Syltherm 800/ferrofluid	Syltherm 800/graphene	Syltherm 800
Solar collectors	683	674.3	675.2
ORC turbine	17.57	17.67	17.67
ORC pump	0.083	0.083	0.083
ORC evaporator	33.96	33.49	33.33
ORC condenser	19.93	20.63	20.58
ARS evaporator	39.3	39.94	39.59
ARS condenser	2.281	2.979	2.927
Absorber	12.995	13.64	13.42
Solution pump	0.005	0.00477	0.00477
ARS generator	45.28	46.07	46.12

the system's overall performance. The greatest exergy destruction occurs in the solar collectors using the Syltherm 800/ferrofluid, at approximately 683 kW of exergy (80%). In comparison with solar collectors, other components showed substantially lower exergy destruction values. The ARS generator destroys 45.28 kW exergy (5%), the ARS evaporator destroys 39.3 kW exergy (4.5%), and the ORC evaporator destroys 33.96 kW exergy (4%). Conversely, the highest values of these components were obtained when Syltherm 800/graphene nanofluid was applied. A major reason behind such a remarkable difference in exergy destruction is a substantial temperature difference among the mentioned components, especially in the solar collector; therefore, while designing solar-trigeneration systems, the solar collector requires careful design because it is the most important component.

To investigate the possibility of improving the system, the effects of certain variables on the overall system performance were studied. Ambient temperature, solar irradiation, and solar collector inlet temperature are considered as the key variables in the system performance. The effects of the mentioned variables on system performance were evaluated in detail under the following baseline conditions: $G_B = 0.96 \text{ kW/m}^2$, $\varphi = 6\%$, ORC turbine inlet pressure is 2000 kPa, and R601 as a working fluid in the ORC.

Effects of solar irradiation

The solar radiation intensity has a significant impact on the PTSC outlet temperature, exergy destruction, and both exergy and energy efficiencies of different working fluids, which are presented in figs. 3 and 4. For evaluating the solar radiation effect on the solar collector outlet temperature, ferrofluid and graphene nanoparticles were used in three different base fluids (Syltherm 800, Therminol VP-1, and Therminol-XP), as fig. 3 shows. The solar collectors' outlet temperature increases when solar irradiation increases. In case of solar collectors, the highest outlet temperature values were obtained using Syltherm 800/graphene as a working fluid. It is so because Syltherm 800/graphene nanofluid has relatively low specific heat capacity and high density as compared to other nanofluids. On the other hand, the lowest values were obtained using the Therminol-XP/ferrofluid as a working fluid in the solar cycle. Since Syltherm 800 has the best thermal properties of all the thermal oils used in this analysis, it has been used as the base fluid for this study.

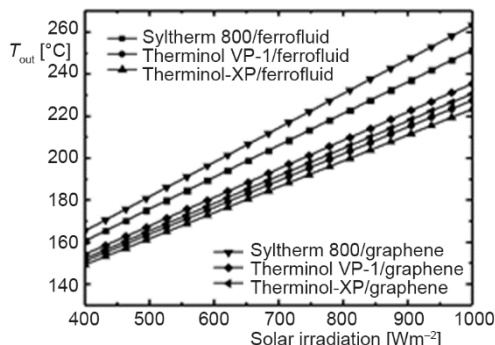


Figure 3. Effect of solar irradiation on the outlet temperature of solar collector

Figure 4 illustrates the solar-trigeneration system's exergy and energy efficiencies for several solar irradiation values using different nanofluids. It clearly shows that in the system, both exergy and energy efficiencies were higher when Syltherm 800/graphene was applied. It is justifiable because high density, relatively low specific heat capacity, and impressive thermal conductivity of this nanofluid lead to more efficiency because the system efficiently absorbs energy in a solar collector and has high outlet temperature. It can also be observed that solar irradiation rate improves the energy efficiency when both nanofluid types were used while the exergy efficiency increases with increasing solar irradiation rates up to a certain point, after that it decreases with time. The highest exergy efficiency using ferrofluid

is 20.12% for solar irradiation close to 935 W and the highest exergy efficiency using graphene is 21.68% for solar irradiation close to 865 W. Figure 4 also shows the solar irradiation effect on a system's total exergy destruction. Obviously, the total exergy destruction increases when the solar irradiation rate spikes.

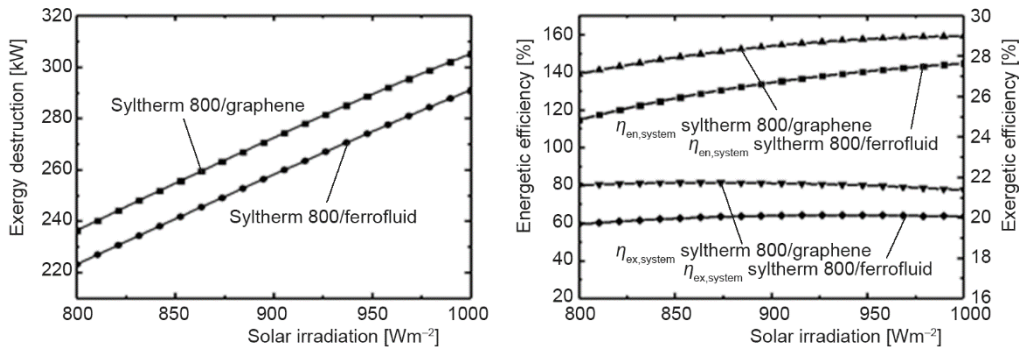


Figure 4. Effect of solar irradiation on overall energy efficiency, overall exergy efficiency, and exergy destruction

Effects of ambient temperature

For analyzing PTSC in greater depth, the ambient temperature effect was studied on the solar collector outlet temperature and efficiency. Their impact on the system's total exergy and energy efficiencies was also studied. It is obvious in fig. 5 that when the ambient temperature surged, the collector efficiency improved. This figure shows very little effect of ambient temperature on the solar collector outlet temperature because the collector temperature rises by a very small amount by increasing the temperature of the medium. Ambient temperature affects the proposed system, specifically its exergy and energy efficiencies, as fig. 5 shows. Obviously, the ambient temperature showed no impact on the system's overall energy efficiency. Therefore, the overall energy efficiency remained almost constant despite increasing ambient temperature and irrespective of the nanofluid used for testing. Being inversely proportional to the ambient temperature, the overall exergy efficiency reduces whenever the ambient temperature surges. The highest overall energy and exergy efficiency values were achieved using graphene nanoparticles in Syltherm 800.

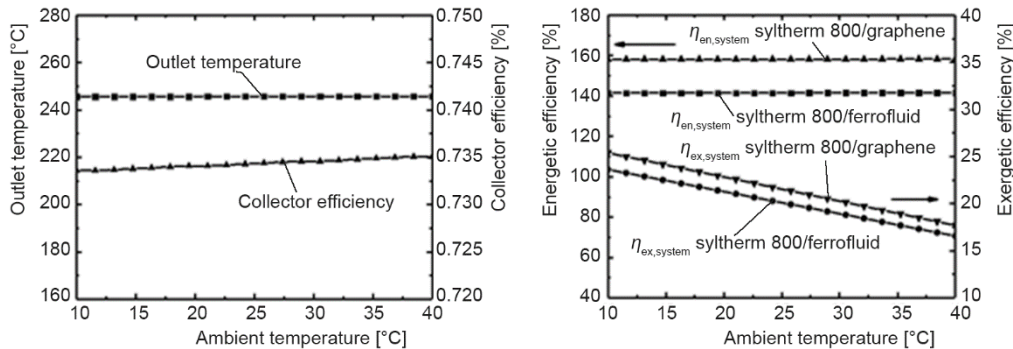


Figure 5. Effect of ambient temperature on collector outlet temperature, collector efficiency, and overall energy and exergy efficiencies

Effects of inlet temperature

For investigating the nanoparticle concentration effect and the PTSC inlet temperature impact on entropy generation, concentration ratios 0.01, 0.05, and 0.1, inlet temperatures 50 °C to 250 °C, and nanofluid Syltherm 800/ferrofluid were considered. Figure 6 shows that at a given flow rate (3 m³), entropy generation rate dropped along with spike in the PTSC inlet temperature. Furthermore, entropy generation surged along with increasing nanoparticle volume concentration. High nanoparticle concentration means higher heat flux inside the absorber tube, higher nanofluid temperature, and surged heat transfer irreversibility. The decrease in entropy generation is followed by inlet temperature increase, which happens because of changes in the nanofluids' thermal properties. An upsurge in temperature reduces the nanofluid density and makes it less viscous; consequently, it decreases the irreversibility of the nanofluid friction.

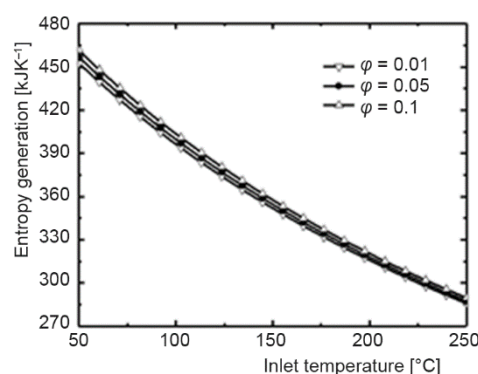


Figure 6. Effect of inlet temperature of PTSC and concentration ratios on entropy generation

Conclusions

In this study, a thermodynamic analysis was performed to study the impact and feasibility of using nanofluids as heating fluids in an integrated PTSC with an ORC and an AHP. The subsystems are operated independently using the same heat source that operates through the switch mechanism. The main functions of the integrated system are cooling, heating system components and providing electricity. The study considered three different types of absorption fluid (Syltherm 800/ferrofluid, Syltherm 800/graphene and Syltherm 800) for the solar cycle and four organic fluids (R123, R401a, R601, and R601a) for the ORC. The performance parameters of the thermodynamic analysis of the base case of an integrated solar-trigeneration system were calculated. Then, some variable parameters were checked separately to determine their impact on system performance. The analyses were performed by the EES software under steady-state conditions. The obtained results indicated that graphene nanoparticles were better than ferrofluid nanoparticles and Syltherm 800 was the best base fluid. Furthermore, R601a was found to be the best organic fluid in comparison with the other fluids studied. The summary of the main conclusions is given below as follows.

- The highest outlet temperature of the PTSC is achieved using Syltherm 800/graphene as a working fluid in the solar cycle at 257.4 °C. This result was accomplished thanks to graphene nanoparticles, which despite their relatively low density have relatively high thermal capacity and thermal conductivity.
- The PTSC with Syltherm 800/graphene have the lowest entropy generation rate value at approximately 438.5 Wm⁻¹K⁻¹ and the lowest exergy destruction rate. This means that the course of this cycle includes the smallest temperature difference and the least irreversibility, which occurs because of the influence of graphene nanoparticles.
- The coefficient of convective heat transfer within the PTSC receiver surged because of nanoparticles. The highest value recorded with a Syltherm 800/ferrofluid was approximately 671.9 Wm⁻²K⁻¹, while was 628.4 Wm⁻²K⁻¹ with Syltherm 800/graphene.

- The highest values of overall energy and exergy efficiencies of the system were achieved using Syltherm 800/graphene as the absorption fluid in the solar system, and R601a as the working fluid of the ORC at 160.5% and 21.84%, respectively.
- The overall energy efficiency value exceeds 100% because the cooling load in the AHP acts as an input into the system along with solar energy and it can be converted to heating production.
- The PTSC using Syltherm 800/ferrofluid are the main exergy destruction source and estimated at 683 kW, which about 80% of the total exergy losses. This is confirmed by the fact that the ferro-fluid nanoparticles have a relatively low specific heat and very high density, which reduces the amount of energy required to raise the temperature. For improving the system performance, careful design process is essential. The improved solar collector design primarily involves higher optical efficiency and low heat loss from the receiver tube.

Nomenclature

A	– area [m^2]	con	– condenser
C_p	– specific heat capacity [$\text{Jkg}^{-1}\text{K}^{-1}$]	en	– energy
\dot{E}_x	– exergy rate [kW]	ex	– exergy
F_R	– heat removal factor	eva	– evaporator
G_B	– solar irradiation [Wm^{-2}]	g	– glass cover
h	– enthalpy [kJkg^{-1}]	gen	– generator
k	– thermal conductivity [Wm^{-2}]	i	– inner
\dot{Q}	– heat transfer rate [kW]	in	– input
S	– absorbed radiation [Wm^{-2}]	nf	– nanofluid
U_L	– heat loss coefficient [$\text{Wm}^{-2}\text{k}^{-1}$]	np	– nanoparticle
W	– work [kW]	opt	– optical

Greek letters

β	– ratio of nanolayer thickness to initial radius of particle	sol	– solar
η	– efficiency	tur	– turbine
μ	– viscosity [$\text{kgm}^{-1}\text{s}^{-1}$]	u	– useful
ρ	– density [kgm^{-3}]		
φ	– nanoparticle volume concentration		

Subscripts

abs	– absorber
amb	– ambient
bf	– base fluid

Acronyms

AHP	– absorption heat pump
CCHP	– combined cooling, heating, power
ORC	– organic Rankine cycle
PTSC	– parabolic trough solar collector
SDC	– solar dish collector

References

- [1] Wang, H., et al., Design Study of Configurations on System COP for a Combined ORC (Organic Rankine cycle) and VCC (Vapor Compression Cycle), *Energy*, 36 (2011), 8, 4809-4820
- [2] Schenk, H., et al., Energetic Comparison of Linear Fresnel and Parabolic Trough Collector Systems, *J. Sol. Energy Eng.*, 136 (2014), 4, 041015
- [3] Zhao, L., et al., Solar Driven ORC-Based CCHP: Comparative Performance Analysis Between Sequential and Parallel System Configurations, *Appl. Therm. Eng.*, 131 (2018), Feb., pp. 696-706
- [4] Al-Sulaiman, F. A., et al., Performance Assessment of a Novel System Using Parabolic Trough Solar Collectors for Combined Cooling, Heating, and Power Production, *Renew. Energy*, 48 (2012), Dec., pp. 161-172
- [5] Olia, H., et al., Application of Nanofluids in Thermal Performance Enhancement of Parabolic Trough Solar Collector: State-of-the-Art, *Appl. Sci.*, 9 (2019), 3, 463

- [6] Ceylan, İ., Ergun, A., Thermodynamic Analysis of a New Design of Temperature Controlled Parabolic Trough Collector, *Energy Convers. Manag.*, 74 (2013), Oct., pp. 505-510
- [7] Bellos, E., et al., Exergetic, Energetic and Financial Evaluation of A Solar Driven Absorption Cooling System with Various Collector Types, *Appl. Therm. Eng.*, 102 (2016), June, pp. 749-759
- [8] Kaya, M., et al., Performance Analysis of Using CuO-Methanol Nanofluid in A Hybrid System with Concentrated Air Collector and Vacuum Tube Heat Pipe, *Energy Convers. Manag.*, 199 (2019), Nov., 111936
- [9] Abid, M., et al., Solar Assisted Multi-Generation System Using Nanofluids: A Comparative Analysis, *Int. J. Hydrogen Energy*, 42 (2017), 33, pp. 21429-21442
- [10] Toghyani, S., et al., Thermodynamic Analysis and Optimization of an Integrated Rankine Power Cycle and Nano-Fluid Based Parabolic Trough Solar Collector, *Energy Convers. Manag.*, 121 (2016), Aug., pp. 93-104
- [11] Alashkar, A., Gadalla, M., Thermo-Economic Analysis of an Integrated Solar Power Generation System Using Nanofluids, *Appl. Energy*, 191 (2017), Apr., pp. 469-491
- [12] Bellos, E., Tzivanidis, C., Optimization of a Solar-Driven Trigeration System with Nanofluid-Based Parabolic Trough Collectors, *Energies*, 10 (2017), 7, 848
- [13] Alashkar, A., Gadalla, M., Performance Analysis of an Integrated Solar-based Power Generation Plant Using Nanofluids, *Int. J. Energy Res.*, 42 (2018), 9, pp. 2875-2900
- [14] Alsaady, M., et al., An Experimental Investigation on the Effect Of Ferrofluids on the Efficiency of Novel Parabolic Trough Solar Collector under Laminar Flow Conditions, *Heat Transf. Eng.*, 40 (2019), 9-10, pp. 753-761
- [15] Khosravi, A., et al., Numerical Analysis of Magnetic Field Effects on the Heat Transfer Enhancement in Ferrofluids for a Parabolic Trough Solar Collector, *Renew. Energy*, 134 (2019), Apr., pp. 54-63
- [16] Pop, E., et al., MRS Bull. 37, 1273 (2012) Pop/Varshney/Roy, *MRS Bull.*, 37 (2012), 12, pp. 1273-1281
- [17] Natividade, P. S. G., et al., Experimental Analysis Applied to an Evacuated Tube Solar Collector Equipped with Parabolic Concentrator using Multilayer Graphene-Based Nanofluids, *Renew. energy*, 138 (2019), Aug., pp. 152-160
- [18] Klein, S. A., F-Chart Software, Engineering Equation Solver, EES Manual; Chapter 1: Getting Started, *Sol. Energy Lab. Univ. Wisconsin-Madison Madison, WI, USA*, (2013)
- [19] Pop, E., et al., Thermal Properties of Graphene: Fundamentals and Applications, *MRS Bull.*, 37 (2012), 12, pp. 1273-1281
- [20] Pekmen Geridonmez, B., Numerical Investigation of Ferrofluid Convection with Kelvin Forces and Non-Darcy Effects, *AIMS Math.*, 3 (2018), 1, pp. 195-210
- [21] Liu, G.L., et al., Selection of Working Fluids for Different Temperature Heat Source Organic Rankine cycle, *Adv. Mater. Res.*, 614-615 (2012), Dec., pp. 195-199
- [22] Chauhan, A., Vaish, R., Fluid Selection of Organic Rankine cycle Using Decision Making Approach, *J. Comput. Eng.*, 2013 (2013), ID 105825
- [23] Kalogirou, S. A., *Solar Energy Engineering: Processes And Systems*, Academic Press, New York, USA, 2013
- [24] Kasaeian, A. B., Convection Heat Transfer Modeling of Ag Nanofluid Using Different Viscosity Theories, *IJUM Eng. J.*, 13 (2012), 1
- [25] Yu, W., Choi, S. U. S., The Role of Interfacial Layers in the Enhanced Thermal Conductivity of Nanofluids: A Renovated Maxwell Model, *J. nanoparticle Res.*, 5 (2003), 1-2, pp. 167-171
- [26] Duangthongsuk, W., Wongwises, S., An Experimental Study on the Heat Transfer Performance and Pressure Drop of TiO₂-Water Nanofluids Flowing Under a Turbulent Flow Regime, *Int. J. Heat Mass Transf.*, 53 (2010), 1-3, pp. 334-344
- [27] Çengel, Y. A., Boles, M. A., *Thermodynamics: An Engineering Approach*, -PDF, McGraw-Hill, New York, USA, 2008
- [28] Bellos, E., Tzivanidis, C., Parametric Analysis and Optimization of a Solar Driven Trigeration System Based on ORC and Absorption Heat Pump, *J. Clean. Prod.*, 161 (2017), Sept., pp. 493-509